Quantum Electronics **49** (4) 399–403 (2019)

FIBRE OPTICS

https://doi.org/10.1070/QEL16922

Method for manufacturing a fibre reflection interferometer based on a metal-dielectric diffraction structure

V.S. Terentyev, V.A. Simonov, I.A. Lobach, S.A. Babin

Abstract. **A new method for manufacturing a two-mirror reflection fibre interferometer in a single-mode fibre consisting of an input mirror with an asymmetric reflection coefficients and a highly reflective end mirror is presented and experimentally demonstrated. The input mirror is based on a metal-dielectric diffraction structure in the form of an aperture in an aluminium film and a dielectric multilayer coating, which provides asymmetry of the reflection coefficient. The method includes the calculation of the energy coefficients of the aluminium film with a hole, the determination of the optimal diameter of the hole, as well as making of the hole, the entrance mirror and the resonator with a short fibre base. A sample interferometer is demonstrated that has an increased (at least by two orders of magnitude) radiation resistance compared to variants based on a continuous metal film, namely, at least 100 mW of radiation in a single-mode SMF-28e fibre at a wavelength of 1550 nm.**

Keywords: *reflection fibre interferometer, aluminium film with a hole, dielectric interference coating, diffraction.*

1. Introduction

A reflection interferometer (RI) is a variant of a multiple-beam two-mirror interferometer. The principal difference between the RI resonator and Fabry–Perot interferometers (FPIs) or Gires-Tournois interferometers is the presence of losses at the input mirror. This makes the reflection characteristic of the RI similar to the FPI transmission function, which can be used for narrow-band filtering of radiation in reflection optical schemes. In addition, RIs have other properties of an FPI: the free spectral region (FSR) varies widely, the response function has high contrast; it is possible to rearrange the reflection peak quickly over the entire FSR. These and other properties allow the use of RIs for the selection of wavelengths in lasers [1]. For fibre optics, the fibre-optic RI is of particular value, making it possible to obtain single-frequency or multi-wavelength generation in fibre or waveguide lasers [2, 3] and to produce coherent wavelength-tunable sources in a wide spectral range. With proper development of technology, as well as depending on the problems solved, fibre RI can compete with modern technologies for the selection of laser radiation, since it has flexible characteristics. For example, it can combine a degree of filtration in reflected light comparable to that of a fibre Bragg grating (FBG) [4], a wide range of radiation tuning (up to 100 nm at a wavelength of 1550 nm), exceeding the maximum spectral range of a FBG (up to 50 nm), as well as a high scanning frequency (over 1 kHz). When the base length is increased in combination with FBG, it is possible to obtain compact reflectors with an ultra-small width of the reflection peak (less than 1 pm), which is practically difficult to achieve in FBG [5]. Based on reflection, RIs can be used in ultrashort (less than 1 mm) laser diode resonators to obtain single-frequency lasing with broadband fast spectral rearrangement without the use of microlenses [6]. For fibre applications, the fibre RI design is simpler than systems based on ring microresonators [7]. It is easier to control fibre RIs compared to multiresonator devices based on the Vernier effect [8], since there is only one controllable parameter (for example, voltage on a piezoceramic actuator) that changes the phase incursion (distance) between mirrors. In addition, the RI response function has high contrast throughout the entire FSR, which is unattainable when using the Vernier method. In particular, this leads to the appearance of parasitic peaks, which can contain up to half the total energy.

To obtain a narrow peak in the reflected light, the input mirror of the fibre RI should have a large asymmetry of the reflection coefficients (the so-called asymmetric mirror) and finite transmission. This is achieved by introducing losses into the dielectric multilayer mirror using a thin metal film, metal or dielectric diffractive structure [5, 9, 10]. At the moment, for practical applications at an acceptable level, only a technology based on a thin metal film has been developed, whose significant drawback is low radiation resistance (about 1 mW at a wavelength of 1550 nm [5, 11]). This makes it difficult to use films for the selection of laser modes with higher power. Calculations show that a significant increase in radiation resistance requires the use of diffraction structures at the fibre end with characteristic dimensions of several micrometres and high manufacturing accuracy [9, 10]. For practical implementation, it is required to develop a technological method for manufacturing such scattering structures and to fabricate on their basis an asymmetric mirror of the RI [11].

The purpose of this work is to demonstrate a new method for manufacturing a fibre metal-diffraction reflection interferometer (FMDRI) for the spectral ranges S, C, and L (1460–1625 nm), which are especially important for optical communication. It was experimentally shown that the threshold of the radiation resistance of the developed FMDRI exceeds 100 mW of continuous radiation at a wavelength of 1550 nm. In this case, a component of an FMDRI is a mirror

V.S. Terentyev, V.A. Simonov Institute of Automation and Electrometry, Siberian Branch, Russian Academy of Sciences, prosp. Akad. Koptyuga 1, 630090 Novosibirsk, Russia; e-mail: terentyev@iae.nsk.su;
I.A. Lobach, S.A. Babin Institute of Automation and Electrometry, Siberian Branch, Russian Academy of Sciences, prosp. Akad. Koptyuga 1, 630090 Novosibirsk, Russia; Novosibirsk State University, ul. Pirogova 1, 630090 Novosibirsk, Russia

Received 29 November 2018; revision received 18 January 2019
Kvantovaya Elektronika **49** (4) 399–403 (2019)
Translated by V.L. Derbov

asymmetrical with respect to reflection coefficients, based on an aluminium film with a hole and a matched dielectric multilayer coating.

2. Calculation part

The schematic of the proposed FMDRI is presented in Fig. 1. Its design is typical for all types of the fibre RI. The end mirror M2 with a reflection coefficient close to unity is formed on one end of a single-mode fibre base. The input mirror M1 located at the end of the left fibre has a more complex metal–dielectric structure. It always includes an element that introduces a loss, which is located on the side of light incidence before the dielectric multilayer coating. In the general case, this leads to the inequality (asymmetry) of the coefficients R_1 and R_2 of reflection into the fundamental mode of the fibre (in particular, one can make $R_1 \ll R_2$). The dielectric coating layers of mirror M1 can have a quarter-wavelength optical thickness (as in a conventional high-reflection mirror [9]), which requires monitoring the sputtering process, i.e., determining the moment of the dielectric change by tracing the reflection from an additional fibre 'witness mirror'. This control is complicated in sputtering systems with high spatial inhomogeneity, e.g., in a magnetron system. In this case, it is impossible to achieve full zeroing of the coefficient R_1, although it can be made sufficiently small. For this reason, in the present work, we use another method of sputtering control based on measuring the reflection coefficient R_1 directly from mirror M1. Then the dielectric layers are not quarter-wavelength ones [2]; however, using this technique R_1 can be almost completely zeroed. In addition, this method does not require a 'witness mirror'.

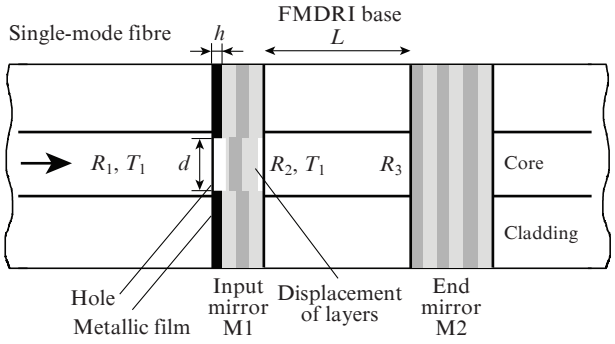

Figure 1. FMDRI optical scheme:
R_1, R_2, and T_1 are the coefficients of reflection and transmission to the fundamental mode of the fibre for mirror M1; R_3 is the reflection coefficient for mirror M2; L is fibre base length; h is the thickness of the metal film; d is the diameter of the hole.

The large asymmetry of the reflection coefficients of mirror M1 ($R_2 \gg R_1 \to 0$, transmission coefficient $T_1 > 0$) leads to the appearance of a 'non-inverted' spectral behaviour of the RI in reflected light, demonstrating narrow peaks on a dark background. For the proof, we consider the expression for the amplitude reflection coefficient r in the plane-wave approximation, which fairly well describes the spectral characteristics of the FMDRI:

$$r = r_1 + \frac{t_1 t_2 r_3 \exp(-\mathrm{i}2\psi)}{1 - r_2 r_3 \exp(-\mathrm{i}2\psi)}, \qquad (1)$$

where the amplitude coefficients of the mirrors $r_j = \sqrt{R_j}\exp(\mathrm{i}\Psi_j)$, $t_j = \sqrt{T_j}\exp(\mathrm{i}\Phi_j)$, $t_1 \equiv t_2$ ($j = 1,2$ for different sides of mirror M1, $j = 3$ for M2) are expressed in terms of the energy coefficients R_j and T_j of reflection and transmission into the fundamental mode of the fibre and their phases Ψ_j and Φ_j; $\psi = 2\pi Ln/\lambda$; L is the length of the fibre segment between M1 and M2; and n is the effective refractive index for the fundamental mode of the fibre. From Eqn (1) it follows that when $R_1 \to 0$, the reflection coefficient $R = |r|^2$ tends to a function similar to the transmission function of the FPI, and when $R_1 > 0$, the form of the response function becomes asymmetric if the combination of phases is $\Psi_1 + \Psi_2 - 2\Phi_1 \neq m\pi$ (m is an integer).

To increase the radiation resistance, it is necessary to use a diffraction structure instead of a continuous film in order to redistribute the major part of the loss from absorption to scattering. The simplest structure for these purposes is a hole of a certain diameter centrally symmetric about the axis of single-mode fibre in an opaque metal film on the end, on which a dielectric coating matched in wavelength is applied [9]. For SMF-28e type fibres, the characteristic hole diameters are 6–7 μm; the film metal should be highly reflective at a wavelength of 1550 nm (e.g., aluminum, silver, or gold). Since dielectric layers are applied on top of a film with a hole, the thickness of the metal layer should be as small as possible so that the displacement of the dielectric layers (see Fig. 1), leading to a decrease in the reflectance R_2 due to diffraction, is minimal.

A high reflection coefficient of the metal film is necessary to minimise the ohmic loss of light energy in the film. Thus, for an aluminium layer with a thickness of 30 nm, the absorption coefficient (at 1550 nm) for a travelling light wave is about 5% according to Ref. [12], which is significantly lower than the absorption of a continuous thin nickel film commonly used in fibre optic with an absorbing film. For a free nickel film, ohmic losses are about 30%, and in the structure of a highly reflective asymmetric mirror, they can exceed 90%. If the centre of the round hole coincides with the point of maximum intensity of the fundamental mode, then the descending wings of the mode intensity distribution fall on the area of the metal film. As a result, the radiation resistance of such a mirror may increase by several orders of magnitude.

There are several methods for making holes of several micrometres. The most accurate of them is laser and other types of lithography [13], capable of making holes of a given and regular shape, including non-circular ones. Using the femtosecond ablation method, which does not require chemical reagents, it is possible to make round holes [14]. The simplest method is laser thermal evaporation [15], the main drawback of which is the formation of characteristic 'collars' of a melt or metal oxide around the perimeter of the hole, which can affect the operation of the RI. The method of thermal laser evaporation of aluminium was chosen because of its greatest practical availability and simplicity.

To estimate the optical parameters of the aluminium film and the degree of its coordination with the dielectric multilayer coating, we calculated before the experiments the optical parameters of the film according to the method [9]. The overlap integral of the field of the fundamental mode of the fibre with the spatial distribution of the reflection and transmission coefficients of the mirror in the form of a metal (Al) film with a hole at the fibre end was calculated and the coefficients of reflection $R_{1,2}^{\mathrm{Al}}$ and transmission T_1^{Al} of such a structure for the fundamental mode of the fibre were found.

Figure 2 shows the calculated dependences of these coefficients for an aluminium film with a thickness of 30 nm at the end of the SMF-28e fibre on the hole diameter d at a wavelength of 1550 nm. As d increases, the reflection coefficients decrease, and R_1^{Al} decreases to zero [dashed line (*4*)] at d = 10.3 μm, i. e., with the hole diameter almost equal to the diameter of the fundamental mode (10.4 μm). Thus, by specifying the reflection coefficient R_1^{Al}, it is possible to determine with some accuracy the diameter of the hole needed to apply a matched dielectric coating and create an asymmetric mirror M1. In addition to the dependence of the transmittance T_1^{Al} for the fundamental mode, Fig. 2 also shows the transmittance T_f^{Al}, which is integral over all modes, from which it is also possible to determine the hole diameter by measuring the fraction of light passed through the hole with a photodetector.

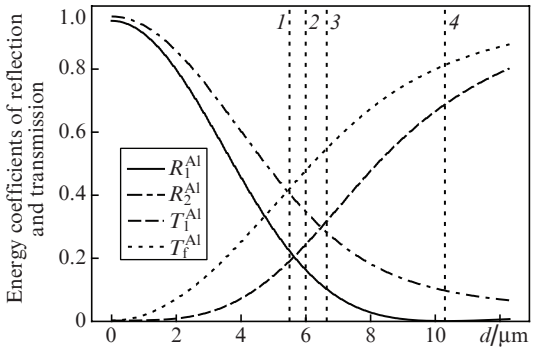

Figure 2. Dependence of the energy coefficients of the aluminium film at the fibre end on the hole diameter d at a wavelength of 1550 nm (film thickness is 30 nm). The vertical dashed lines correspond to d = (*1*) 5.5, (*2*) 6, (*3*) 6.65 and (*4*) 10.3 μm.

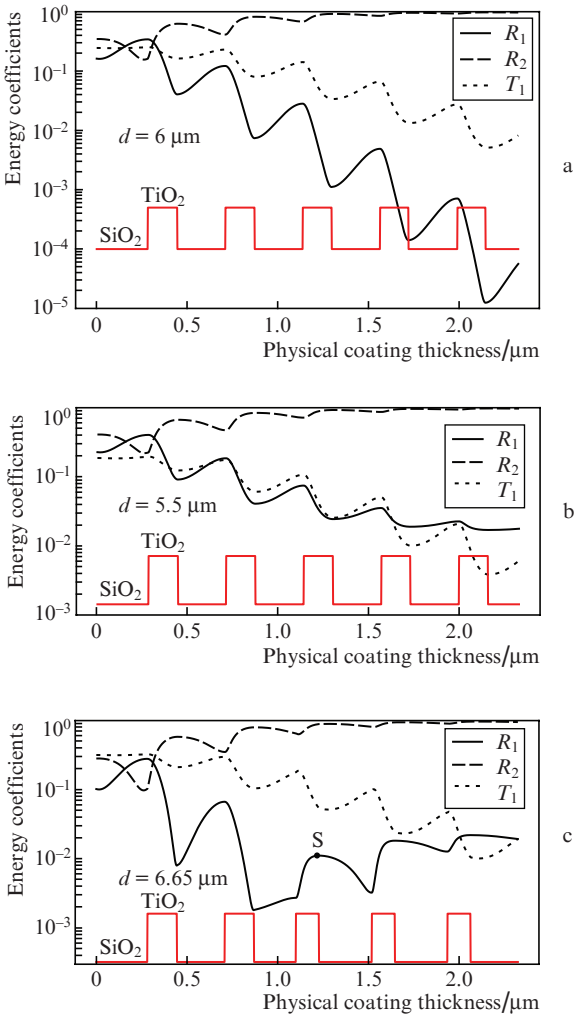

Figure 3. Modelling the process of sputtering a dielectric multilayer coating on an aluminium film with a thickness of 30 nm for d = (a) 6, (b) 5.5 and (c) 6.65 μm. The meander-shaped line shows the deposition areas of dielectrics with high (TiO_2) and low (SiO_2) refractive indices.

The vertical lines (*1*, *2*, *3*) in Fig. 2 indicate the diameters for which the behaviour of the energy coefficients R_1, R_2, and T_1 of the mirror M1 (Fig. 3) is plotted during the deposition of dielectric films of oxides of titanium (TiO_2) and silicon (SiO_2) on the film with a hole. The change of dielectric was controlled by the extrema of R_1, which do not always coincide with the extrema of T_1. Figure 3a shows the case of optimal matching (d = 6 μm), when the coefficient R_1 decreases with increasing thickness of the coating to negligibly small values (less than 10^{-4}). In the case of an asymmetric mirror based on a continuous film, such a value of R_1 corresponds to an optimal nickel film thickness of about 10 nm [16]. If the hole diameter is less than optimal (d = 5.5 μm), R_1 decreases and tends to a certain limit value (about 10^{-2}); this corresponds to the thickness of the continuous nickel film exceeding the optimum (10–20 nm). If the diameter d is larger than the optimum one (6.65 μm, Fig. 3c), then the dependence of R_1 on the coating thickness has a break at a certain point, after which it ceases to decrease (equivalent to the case of a thinner continuous film, 5–10 nm). In all three cases, the transmittance T_1 falls, and R_2 approaches unity; at the same time, the condition $R_1 \ll R_2$ is fulfilled; therefore, depending on the task, a certain finite range of diameters may be suitable near the optimal value.

3. Experimental implementation of the method

The method of manufacturing FMDRI can be divided into three stages. At the first stage, the ends of fibre ferrules with fibres fixed in them were polished and placed in a vacuum magnetron sputtering system, where an aluminium film about 30 nm thick was deposited. The deposition was carried out in a voltage-stabilised pulse magnetron discharge with a 10% filling factor at a voltage of 1000 V, a current of 0.3 A, a pulse repetition rate of 29 kHz, and an argon pressure of 10^{-3} mm Hg.

At the second stage, holes were made in the films, and their radiation resistance was checked at the facility shown in Fig. 4a using a cw Er^{3+} fibre laser with a generation wavelength of 1600 nm, specified by the FBG. The pump laser diode current increased in such a way that the resulting small aperture was in the spatial region near the maximum mode intensity. Unfortunately, noises of various nature (electronic, acoustic), affecting the stability of the intensity of the radiation of a fibre laser, led to rapid and poorly controlled evaporation of the film with the formation of a hole having a diameter from 8 to 10 μm. Using a Coherent PowerMax PS10 power meter (PD1 in Fig. 4a), the power of the radiation transmitted through the film and the transmittance T_{P1} of the film (corresponding to T_f^{Al} in Fig. 2) were determined, and using the Thorlabs S122B meter (PD2) the power of radiation reflected into the fundamental mode of the fibre and the ref-

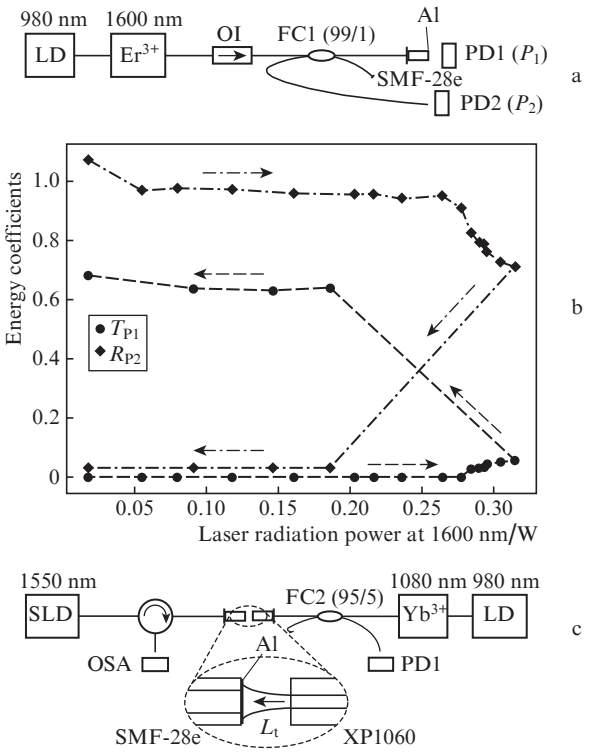

Figure 4. Experimental implementation of the method of thermal evaporation of an aluminium film: (a) schematic of measuring the radiation resistance of the film [(LD) pumping laser diode, (OI) optical isolator, (FC1) fibre coupler 99/1 (1550 nm), (PD1) and (PD2) meters of powers P_1 and P_2]; (b) dependences of the coefficients of transmission T_{P1} and reflection R_{P2} of the film on the laser radiation power (the arrows indicate the sequence of changes in the erbium laser power); (c) setup for making a hole in a film using a fibre Yb^{3+} laser (1080 nm) [(SLD) superluminescent diode (1550 nm), (FC2) fibre coupler 95/5 (1060 nm), (OSA) optical spectrum analyser].

lection coefficient R_{P2} (corresponding to R_1^{Al} in Fig. 2) were measured.

Figure 4b shows the dependences of the coefficients T_{P1} and R_{P2} on the power of the Er^{3+} laser typical for all films. It can be seen that with the power increasing above 250–260 mW, the nature of the dependences significantly changes (most often due to the rapid evaporation of the film), but sometimes (in the power range 250–320 mW), they are observed to change slowly. In this case, a hole was formed with a small diameter (about 2 μm) (see Fig. 2). After the uncontrolled formation of a hole of larger diameter (more than 8 μm), it was possible to smoothly increase its diameter, raising the radiation power above 320 mW. However, this increased the area of the transition region around the hole consisting of light-scattering formations of molten metal and/or its oxides, which is typical of the thermal evaporation method [15]. The diameter and shape of the holes was monitored using a microscope, the changed diameter values corresponded to the dependence $R_1^{Al}(d)$ shown in Fig. 2.

To make holes with diameters in the region near 6 μm, bounded by lines (*1*) and (*3*) (Fig. 2), it is necessary to reduce the diameter of the mode of incident radiation. For this purpose, an ytterbium fibre laser with a wavelength of 1080 nm and XP1060 fibre (Nufern) with the fundamental mode diameter (FMD) 6.3 μm were used. To ensure the axial symmetry of the hole in the film deposited on the end of the SMF-28e fibre, the scheme shown in Fig. 4c was exploited. In the air gap between the SMF-28e and XP1060 fibres (see inset), the fundamental Gaussian mode of free space propagated, the outgoing radiation beam expanded, and the spot size on the film could be precisely varied by changing the distance L_t between the fibre ends. The distance L_t was controlled with a Yokogawa AQ6370 optical spectrum analyser (OSA) measuring the spectrum of reflection from the XP1060 face illuminated with a superluminescent diode ($\lambda = 1550$ nm) and using the formula $L_t = \lambda^2/(2\Delta\lambda_t) = 18.4$ μm, where $\Delta\lambda_t = 65.2$ nm is the FSR (the distance between transmission peaks). The radiation power at which the film burned out was about 200 mW. Thus, a hole with a diameter of 6.7 μm was obtained with a reflection coefficient $R_1^{Al} = 0.1$, which approximately corresponds to line (*3*) in Fig. 2. To obtain the optimal hole diameter (6 μm), it is necessary to reduce the diameter of the incident radiation mode, for example, replacing XP1060 fibre with 780HP fibre (Thorlabs), whose FMD is 5.9 μm at 1080 nm, or any other one that has a smaller FMD. However, it is obvious that to achieve greater radiation resistance, it is more advantageous to have a hole of larger diameter.

At the third stage, a dielectric coating was deposited on the fibre end. In this case, a dependence of R_1 on the coating thickness was observed, corresponding to that calculated in Fig. 3c. At point S, the sputtering process was stopped. The measured reflection coefficient at this point R_1^S was 0.002 (the calculated value is approximately 10^{-2}). The deposition process was monitored at a wavelength of 1529.4 nm.

In a separate fibre ferrule, the FMDRI base was formed, consisting of a fibre segment of length $L = 38$ μm and mirror M2 deposited on the end face. The latter consisted of 13 quarter-wavelength layers of TiO_2 and SiO_2. The maximum of the spectral reflection of mirror M2 was at 1529.4 nm, and its reflection coefficient R_3 was taken to equal 0.99.

4. Experimental results

The reflection spectrum of the fabricated interferometer, measured with an OSA with a spectral resolution of 20 pm, is shown in Fig. 5. The FSR of the interferometer is $\Delta\lambda = 21.8$ nm, the finesse is 30.2; hence, using Eqn (1) we obtain the reflection coefficient $R_2^S = 0.82$, which approximately corresponds to its calculated value of 0.88 (see Fig. 3). The maximum reflection coefficient was 0.5 near $\lambda \approx 1529.4$ nm. In the region of longer wavelengths, the maximum value of R_2 increases due to an increase in the reflection coefficient R_1, and the asymmetry of the shape of the response function peaks increases. At a wavelength of 1595 nm, ultralow ($\sim 10^{-5}$) reflection is achieved (it may be even smaller, but the spectrum is limited by the resolution of the OSA). In principle, the reflection coefficient may even be equal to zero due to the complete destructive interference of two waves [see Eqn (1)], which is impossible for an FPI in the transmission regime. Note that the minimum of the reflection coefficient corresponding to the optimal matching is shifted from the wavelength of 1529.4 nm to the shortwavelength region by several nanometres. This may be due to the fact that during the deposition of dielectrics, the surface of the end face contacts with the plasma of the magnetron gas discharge and its temperature in the near-surface region can be hundreds of Celsius degrees. The influence of variation in the thickness of the applied dielectric layers cannot be excluded, too. The response function of the interferometer is quite broadband; such an interferometer can be used to select laser wavelengths at least in the spectral region of 1500–1600 nm (see Fig. 5).

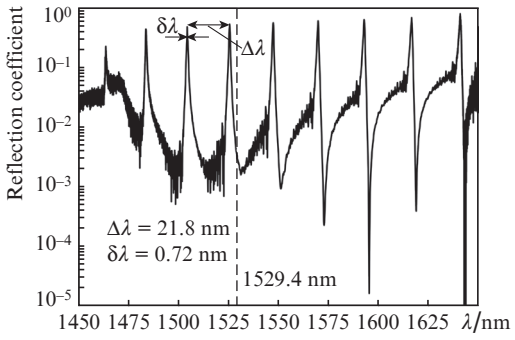

Figure 5. FMDRI reflection spectrum: $\Delta\lambda$ is the FSR of the interferometer; $\delta\lambda$ is the spectral FWHM of the reflection peak.

To record the reflection spectrum, a superluminescent diode with a wavelength of 1550 nm and an integrated power of 7.5 mW was used, which convincingly demonstrates a significant increase in the radiation resistance of the FMDRI in comparison with thin metal film versions. The limiting radiation resistance of the interferometer can be estimated using Fig. 4b, which shows that the aluminium film begins to melt at an incident power of 200–250 mW in the spectral range of 1500–1600 nm.

5. Conclusions

A method for manufacturing a reflection fibre interferometer, made in a single-mode fibre, is described. The radiation resistance of the FMDRI is at least 100 mW at a wavelength of 1550 nm, which is by more than two orders of magnitude better than in reflection interferometers based on a thin metal film. The design of the proposed interferometer includes an asymmetric reflectance mirror based on an opaque aluminium film with a hole and a dielectric multilayer coating. Methods for calculating and manufacturing holes in aluminium film, as well as asymmetric mirrors, are presented. We believe that the use of more highly reflective metals (silver, gold) or radiation in other spectral ranges, where metals have greater reflectivity, will further increase the radiation resistance of the interferometer to cw radiation.

This variant of the interferometer can be used for radiation selection in fibre (waveguide) lasers, e.g., for single-frequency or multiwave radiation selection in fibre continuous-wave lasers with power up to 100 mW, which are of interest for interrogation systems of FBG-based quasi-distributed sensor lines or developing a compact laser spectrum analyser.

The results confirm the operability of the diffraction version of a fibre reflection interferometer and provide confidence in the possibility of producing an asymmetric mirror based on fully dielectric diffraction structures, although this seems to require the use of more complex methods of laser or electron beam lithography.

Acknowledgements. The work was carried out within the State Task for the Institute of Automation and Electrometry of the Siberian Branch of the RAS (No. AAAA-A17-117062110026-3). Experimental studies were carried out using the equipment of the Shared Facilities Centre 'Spectroscopy and Optics' at the Institute of Automation and Electrometry, SB RAS.

The authors are grateful to V.P. Bessmel'tsev for useful discussions of the results of the work.

References

1. Terentyev V.S., Simonov V.A. *Quantum Electron.*, **43**, 706 (2013) [*Kvantovaya Elektron.*, **43**, 706 (2013)].
2. Terentyev V.S., Simonov V.A., Babin S.A. *Opt. Express*, **24**, 4512 (2016), DOI: 10.1364/OE.24.004512.
3. Terentyev V.S., Simonov V.A., Babin S.A. *Laser Phys. Lett.*, **14**, 25103 (2017), http://dx.doi.org/10.1088/1612-202X/aa548e.
4. Kashyap R. *Fiber Bragg Gratings* (Academic Press, 2010), https://doi.org/10.1016/B978-0-12-372579-0.00003-X.
5. Terentyev V.S., Vlasov A.A., Abdullina S.R., Simonov V.A., Skvortsov M.I., Babin S.A. *Quantum Electron.*, **48**, 728 (2018) [*Kvantovaya Elektron.*, **48**, 728 (2018)].
6. Mroziewicz B. *Opto-Electron. Rev.*, **16** (4), 347 (2008), DOI: 10.2478/s11772-008-0045-9.
7. Gorajoobi S.B., Murugan G.S., Zervas M.N. *Opt. Express*, **26**, 26339 (2018).
8. Wang R., Sprengel S., Vasiliev A., Boehm G., Campenhout J.V., Lepage G., Verheyen P., Baets R., Amann M.-C., Roelkens G. *Photon. Res.*, **6**, 858 (2018).
9. Terentyev V.S., Simonov V.A. *Quantum Electron.*, **46**, 142 (2016) [*Kvantovaya Elektron.*, **46**, 142 (2016)].
10. Terentyev V.S., Simonov V.A. *Prikl. Fotonika*, **4**, 107 (2017), DOI: 10.15593/2411-4367/2017.02.03.
11. Terentyev V.S., Simonov V.A., Babin S.A. *Materialy Rossiyskogo seminara po volokonnym lazeram* (*Proceedings of the Russian Seminar on Fibre Lasers*) (Novosibirsk, 2018) p. 132.
12. Rakić A.D. *Appl. Opt.*, **34**, 4755 (1995).
13. Korolkov V.P., Nasyrov R.K., Sametov A.R., Suhih S.A. *Proc. SPIE*, **7957**, 795710 (2011).
14. Dostovalov A.V., Terentyev V.S., Bessmel'tsev V.P. *Prikl. Fotonika*, **4**, 22 (2017), DOI: 10.15593/2411-4367/2017.01.03.
15. Maydan D. *Bell System Techn. J.*, **50**, 1761 (1971), DOI: 10.1002/j.1538-7305.1971.tb02581.x.
16. Kamenev N.N., Troitskii Yu.V. *Opt. Spectrosc.* **54**, 428 (1983) [*Opt. Spektrosk.*, **54**, 725 (1983)].